Vol. 39, No. 4 (2017) 536-546, DOI: 10.24874/ti.2017.39.04.13

Tribology in Industry

www.tribology.fink.rs

RESEARCH

Stability Loss of the Cemented Stem of Hip Prosthesis due to Fretting Corrosion Fatigue

L. Capitanu[a], L.-L. Badita[b], V. Florescu[c]

[a] *Institute of Solid Mechanics of the Romanian Academy, Constantin Mille Str, no. 15, 1st district, Bucharest, Romania,*
[b] *National Institute of Research and Development in Mechatronics and Measurement Technique, Pantelimon Str., no. 6-8, 2nd district, Bucharest, Romania,*
[c] *University of Civil Engineering, Plevnei Way, no. 59, 5th district, Bucharest, Romania.*

Keywords:

Hip prosthesis
Ti6Al4V
Polymetylmethacrilate
Cemented stem
Fretting fatigue corrosion

Corresponding author:

Liliana-Laura Badita
National Institute of Research and Development in Mechatronics and Measurement Technique,
Pantelimon Str., no. 6-8, 2nd district,
Bucharest, Romania.
E-mail: badita_l@yahoo.com

A B S T R A C T

Aim of this project was to study the fretting behaviour of the cemented femoral stem fixation of a total hip prosthesis, trying to capture the loss of contact between the femoral stem and polymetylmethacrilate cement fixation. To have a landmark, studies were performed compared with cementless fixation, where no fretting phenomenon occurs, on real prostheses, under biological 3D loading conditions. A fatigue test device, installed on a servo-hydraulic triaxial dynamic testing machine was used. It allowed monitoring the flexion-extension, abduction-adduction, inner-outer rotation movements, and the variation of the torsional torque, depending on normal loading. The test ends when the sample does not fail after 2000000 cycles, or when it has reached a predetermined number of cycles. Test fluid medium used was NaCl mixed with distilled water, a favourable environment for appearance of fretting corrosion. After the failure of stem fixation at 2450000 cycles, the mantle of bone cement remaining adherent on femoral stem was removed. Microscopic inspection of the femoral stem and of the inner part of the polymetylmethacrilate mantle demonstrated the existence of corrosion of the femoral stem surface beneath the cement mantle, and Fe_2O_3 deposits on the femoral stem surface and on the inner part of the mantle.

1. INTRODUCTION

Fretting refers to the process involving movements of low amplitude, more precisely movements with total amplitude smaller than the width of contact between two components. There are several application areas where this phenomenon occurs, such as aerospace industry, implants in the human body, automotive, etc. In the recent years, several studies have focused on the understanding of this phenomenon, and on finding solutions to prevent and/ or avoid it.

Fatigue design of certain components in these areas, without taking into account the effect of fretting, will certainly lead to premature and unexpected failure in many applications [1]. Fretting corrosion is a degradation phenomenon

of contact in an aqueous medium. It is one of the most critical issues in designing total hip prostheses, since it occurs at the contact surface between femoral stem and bone cement [2]. Fretting in a total hip prosthesis is due to the destruction of the passive oxide on metal, leading to increased corrosion and to the generation of residues, such as polymer and metal oxides particles [3]. This leads to serious dysfunctions of the prosthetic hip joint. Cyclic loading due to human gait and differences between the mechanical properties of the femoral stem and bone cement give rise to loss of contact between the two materials. This leads to secondary effects, such as damage and cracking of cement. Remains, including metal oxides and ions, penetrate the bone tissues through cracks and, finally, induce inflammation of bone tissues. Currently, the most used materials for manufacturing femoral stems are CoCr alloy, Ti alloys or austenitic stainless steels (SS 316L). Bone cement, such as polymetylmethacrilate (PMMA) is introduced into the spongy and the cortical bones. Damage by fretting corrosion between SS 316L femoral stem and PMMA bone cement was experimentally investigated under similar conditions to those found in a real prosthesis [4]. The interfacial energy dissipated and the wear volume, after 2000000 cycles were measured. It has been demonstrated that the wear volume can be expressed as a function of the dissipated interfacial energy. Fretting phenomena have been studied both in air and in aerated solutions. When exposed to air, it was not observed any significant wear on stainless steel, but mechanical wear was found when it came in contact with PMMA. It has been found that the wear volume of PMMA is linearly correlated with the cumulative energy dissipated [5]. Fretting – material's damage caused by small oscillating movements between the bodies in contact – can lead to surfaces deterioration and dimensional changes. A remarkable decrease of the useful life in the presence of bulk effort can also be seen. Surface's damage is defined as the fretting wear, while the development of the crack can be called fretting fatigue [6]. For the life estimation at fretting fatigue, the complete process problems are usually divided into two phases – crack's initiation and crack's propagation. There is still a debate on the proportion of life time taken by these two phases, most of the authors considering both of them in the stage of estimating the total life. Therefore, it still continues the search for more appropriate selection criteria. Each criterion is appropriate in some selected combinations of materials, geometry, type of contact conditions, and loading.

The level of fretting damage is determined by the amplitude of the relative sliding between the femoral stem and bone cement [7]. If the sliding amplitude is so small that some contact parts remain adherent, and others slide over the other opposite surface, the cracks are predominantly generated in the vicinity of the contact edges (fretting fatigue). If the sliding amplitude is large enough to make all the parts of a surface to slide over the other surface, the wear takes place over the entire contact surface (fretting wear). It was identified by numerical modelling, in which the sliding amplitude between the femoral stem and bone cement is about 0.05 mm under the strains applied during normal human gait. It was observed that the sliding amplitude induces the fretting wear in total hip prosthesis. The concentration of chloride (ionic strength), the concentration of protein (albumin) and solution pH could affect the fretting corrosion of materials used in a total hip prosthesis. Influences of ionic strength, of albumin and of the potential applied were studied by fretting corrosion tests using SS 316L and PMMA bone cement. It was established that the ionic strength increases the wear volume on SS 316L at the open circuit potential. Albumin with concentration of 1 gL^{-1} does not play a significant role in determining the total wear volume of SS 316L, compared with albumin of 0 gL^{-1}. At a potential applied E = -0.4 V (SCE), there is a threshold concentration (NaCl solution) of 0.1 M over which the metal dissolution is improved. A concentration of 20 gL^{-1} albumin decreases the wear volume of SS 316L, but increases the wear volume of PMMA [7]. Similar findings were presented and for femoral stems made of Ti6Al4V alloy [8]. In the human body, Ti6Al4V alloy is immersed in a physiological solution having a high concentration of NaCl (~ 0.2 M) at a temperature of 38 °C. Because of the significant difference in mechanical properties (especially Young's modulus, with a ratio of 90 between Ti6Al4V and PMMA) shielding stress occurs. This physical phenomenon can be explained as follows. Metallic materials and polymers do not present the same deformation under applied stress, leading to unsoldering between the metal

and cement. Therefore, the adhesion between metal and polymer loses after a short period of human gait. This unsoldering involves fretting (friction under small displacements) and subsequent friction between materials in contact. Thereafter, Ti6Al4V and the bone cement are subjected to small displacements, friction loadings in a corrosive environment, resulting in fretting corrosion. Consequently, the wear between the bone cement and Ti6Al4V alloy occurs. It involves the generation of debris, which often cause inflammations or reactions, ending with aseptic loosening of implants fixation and the necessity of replacement.

Giannakopoulos et al. [9] stated that the fretting problem can be addressed as a matter of simple fatigue subjected to a localized stress concentration. They developed an analytical model for the fretting fatigue at a corner of a rounded mandrel in contact with a substrate and made an analogy with fatigue crack initiation at the notch of a tip. They analysed the similarities and differences between the stress concentration factors at the edge of the contact mandrel on flat rounded suddenly and the tip of a blunt crack. The methodology analogous to the notch provided a direct connection between the life of fretting fatigue crack initiation of a flat mandrel with rounded corners and the life of simple fatigue crack initiation of a smooth sample of the same material. Model predictions compared with fretting fatigue experiments on Ti6Al4V showed a good concordance.

Fretting fatigue is a type of multiaxial fatigue, having a non-proportional loading, thus introducing multiaxial stress fields and severe stress gradients. Therefore, in order to define the failure, multiaxial criteria are used. In the past, multiaxial criteria that use critical damage parameters have been developed, together with various ways to define the estimated life. Generally, stress and strain components combined with material constants are fully assimilated to the limit of fatigue resistance in tension/ inverted torsion or by Manson-Coffin and Basquin relation [10]. Hence, it allows computing the estimated life time according with the fretting fatigue scenario. Some researchers have used the approach of continuum damage mediums (CDM) mechanics, which is based on thermodynamic potential function and on the fact that crack initiation life can be estimated using bulk materials properties. Based on the approach used to model the initiation of fretting fatigue crack, different criteria can be classified as: critical plane approach, invariant stress approach and CDM approach. The aim of this paper was to study the fretting behaviour of the cemented femoral stem fixation of a Ti6Al4V/ UHMWPE total hip prosthesis. To have a landmark, studies were performed compared with cementless fixation, where no fretting phenomenon occurs. The study was done on real prostheses, under biological 3D loading and motion conditions.

2. MATERIALS AND EXPERIMENTAL TECHNIQUES

2.1 Materials

Typically, the stems of hip prostheses are made of SS 316L, Ti6Al4V or CoCr alloys, because of their mechanical properties and good biocompatibility [1]. In this study, the contact of Ti6Al4V alloy with PMMA was studied, simulating the femoral stem/ fixation material contact. PMMA is a thermoplastic optically transparent material. At room temperature, it is a hard and brittle material. Its mechanical resistance is much smaller than that of Ti6Al4V alloy, so a prosthetic stem made of Ti6Al4V alloy, with chemical composition shown in Table 1, was used.

Table 1. Chemical composition of the Ti6Al4V alloy (w/w).

Elements	Composition
Al	5.60-6.75
O (max)	0.020
N (max)	0.05
V	3.50-4.50
Fe (max)	0.40
St (max)	0.015
H (max)	0.10
Other (max)	0.40
Ti	Balance

Fixation was realized with PMMA bone cement (PMMA Perspex®) whose mechanical properties are shown in Table 2.

Table 2. Mechanical properties of the tested materials.

Mechanical properties	Ti6Al4V	PMMA
Poisson Coefficient (υ)	0.29	0.39
Young modulus (E) [MPa]	119	2.5
Yield strength (σ_c) [MPa]	825	65
Tensile strength (σ_t) [MPa]	805	75

2.2 Experimental devices

Fretting tests were performed on a Instron® device for fatigue testing of the femoral stem cemented fixation of the total hip prosthesis – Fig. 1, installed on a servo-hydraulic multiaxial dynamic testing machine MTS Bionix, equipped with testing system for hip implants – Fig. 2.

(a)

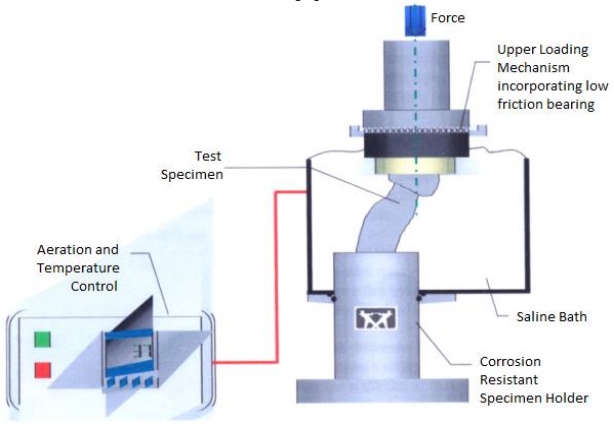

(b)

Fig. 1. (a) Instron® fatigue test device for the femoral stem cemented fixation of the total hip prosthesis, and (b) Instron® testing system scheme for prosthetic stem fatigue fixture.

Instron® device – Fig. 1(a) simulates fatigue loading of a hip cemented stem during a gait cycle. Device consists of a support made of a composite femur model from Sawbones® transparent plastic with intramedullary channel, in which the prosthetic stem is cemented. It has a low friction loading head, incorporating a low friction bearing and an adapter for mounting to the system loading cell – Fig. 1(b). This device is mounted in a sealed saline chamber, which contains a NaCl high concentration solution (~ 0.2 M) at a temperature of 38 °C. The ensemble has a temperature regulator and a circulation pump for in vivo testing. The flexible support for prosthetic stem allows a wide variety of hip geometries, offset angles, materials and embedding depths to be used. The device applies compression, bending and torsion to meet the ISO 7206-4 requirements.

Loading compression through the loading head makes the femoral stem specimen to be subjected to loads and frequencies as specified in ISO 7206-8. The test ends either when the sample does not fail after 2000000 cycles, or when it has reached a predetermined number of cycles. In the case of this research, the test was stopped at 2450000 cycles, when indices of fretting appeared. Test fluid medium used was NaCl mixed with distilled water and testing frequency was 10 Hz.

Fig. 2. MTS Bionix servo-hydraulic multiaxial dynamic testing machine, equipped with system for testing the hip implants.

MTS Bionix servo-hydraulic multiaxial dynamic testing machine (Fig. 2) allows triaxial testing of hip implants and in tribological terms [11].

MTS Bionix system is equipped with three rotating motors for inner-outer rotation (IOR), flexion-extension (FE) and abduction-adduction (AA) movements and with three displacement transducers, one for each type of movement. In addition, it has a transducer for the moment of torsion, with two Wheatstone decks, one for measuring linear force and the other to measure the torsion moment. The moment transducer is of resistive type and it is coupled with a current converter type 662 20 h-04, to process received signals from each Wheatstone deck.

The test machine allowed setting number of cycles, the amount of the normal force on the joint implant (the force *F* that has a pulsating form), the lower and upper limits of the angular displacement of each rotation, as well as the law of motion for each type of rotation according to ISO 14242-3.

Appropriate fitting of the sample was verified before the time of the test. It has been adjusted at the pump pressure value of 210 bar, the controller and the application "Station Manager" were started, by which were made relations to the system calibration settings and adjusted. After that, zero settings had been done. After the command – response adjustments, the output values for each axis (axial, torsion, FE, AA, IOR) have zeroed.

3. EXPERIMENTAL RESULTS AND DISCUSSION

Through the "ELITE" software the vertical push force and the displacement angles were set: FE, AA, IOR, according to ISO 14242 upgraded in 2014, which sets the parameters for orthopaedic implants testing, of the limits 1 and 2.

Values in Table 3 show the force, its maximum amount being 3 kN. The sign is negative because it is a compression force (the negative sense of the z axis).

Values for abduction-adduction, inner-outer rotation and flexion-extension angles are presented in Tables 4, 5 and 6.

After entering values for force and angle of movement in FE, AA, IOR, it was set the number of test cycles to 2000000 cycles.

Table 3. Values for the axial force of pressing.

(1) Channel: Axial; Force measurement (kN)				
Time (sec.)	**Segment count**	**Wave**	**1 Limit (kN)**	**2 Limit (kN)**
0.0005	10000	Sinus	-0.3000	-0.3000
0.1195	10000	Sinus	-3.0000	-1.5000
0.2000	10000	Sinus	-1.5000	-0.3000
0.1800	10000	Sinus	-3.0000	-0.3000
0.1200	10000	Sinus	-3.0000	-0.3000
0.3800	10000	Sinus	-0.3000	-0.3000

Table 4. Values for Abduction-Adduction angle, according to ISO 14242.

(1) Channel: Axial; Force measurement (kN)				
Time (sec.)	**Segment count**	**Wave**	**1 Limit (kN)**	**2 Limit (kN)**
0.0005	1.0000	Sinus	-3.0000	7.0000
0.1195	1.0000	Sinus	7.0000	-4.0000
0.2000	1.0000	Sinus	-4.0000	3.0000
0.3800	1.0000	Sinus	3.0000	3.0000

Table 5. Values for Inner–Outer Rotation angle, according to ISO 14242.

(1) Channel: Axial; Force measurement (kN)				
Time (sec.)	**Segment count**	**Wave**	**1 Limit (kN)**	**2 Limit (kN)**
0.0005	1.0000	Sinus	-10.0000	2.0000
0.5000	1.0000	Sinus	2.0000	-10.0000
0.4995	1.0000	Sinus	-10.0000	-10.0000

Table 6. Values for Flexion-Extension angle, according to ISO 14242.

(1) Channel: Axial; Force measurement (kN)				
Time (sec.)	**Segment count**	**Wave**	**1 Limit (kN)**	**2 Limit (kN)**
0.0005	1.0000	Sinus	25.0000	-18.0000
0.5000	1.0000	Sinus	-18.0000	25.0000
0.4995	1.0000	Sinus	25.0000	25.0000

For MTS Bionix system calibration, the prosthesis was subjected to simultaneous requests of FE, AA and IOR during a cycle and was considered a time of 5 seconds, where human subject achieves 5 complete cycles. In Figure 3 are shown the graphs of vertical contact force: the answer come from the force transducer is represented by the red colour and blue is the command set.

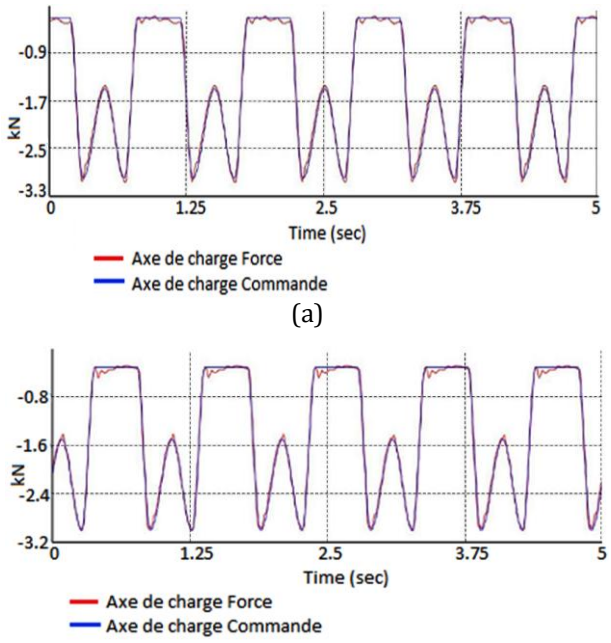

Fig. 3. Time graph of the vertical contact force, command-response (blue-red) when testing the cemented prosthesis (a) and (b) a cementless prosthesis (press-fitted stem).

In time graph of the vertical contact force and angular displacement of the flexion-extension (Fig. 4) is presented for a cemented prosthesis (a) and (b) a cementless prosthesis.

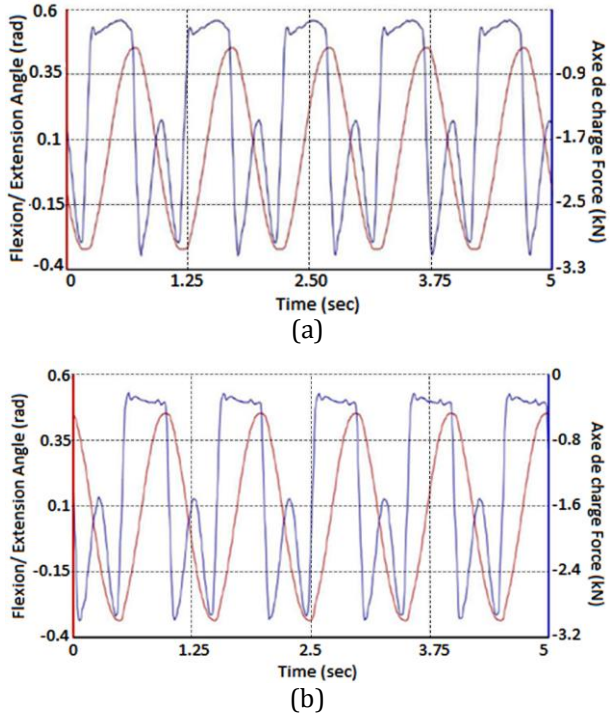

Fig. 4. In time graph of the vertical contact force and angular displacement of the flexion-extension when testing the cemented prosthesis (a) and (b) a cementless prosthesis.

At the same time, the graph of the vertical contact force and angular displacement of the abduction-adduction (Fig. 5) is presented when testing the cemented prosthesis (a) and (b) a cementless prosthesis.

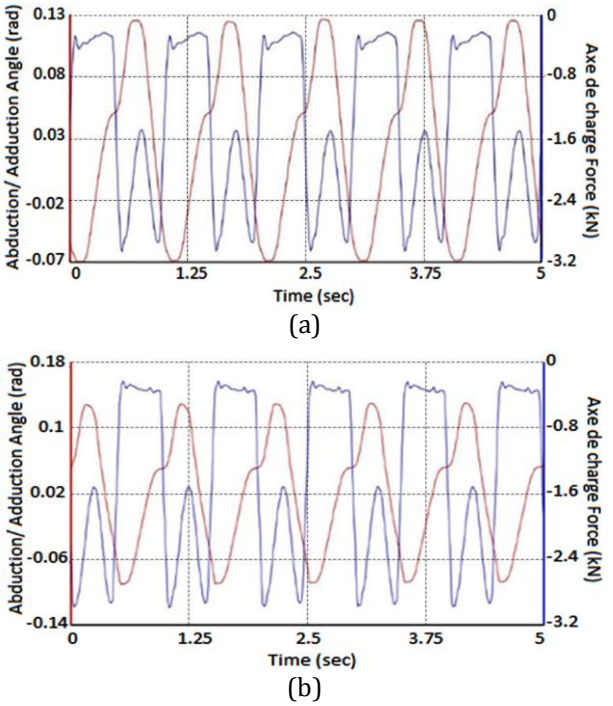

Fig. 5. In time graph of the vertical contact force and angular displacement of abduction-adduction when testing (a) the cemented prosthesis and (b) a cementless prosthesis.

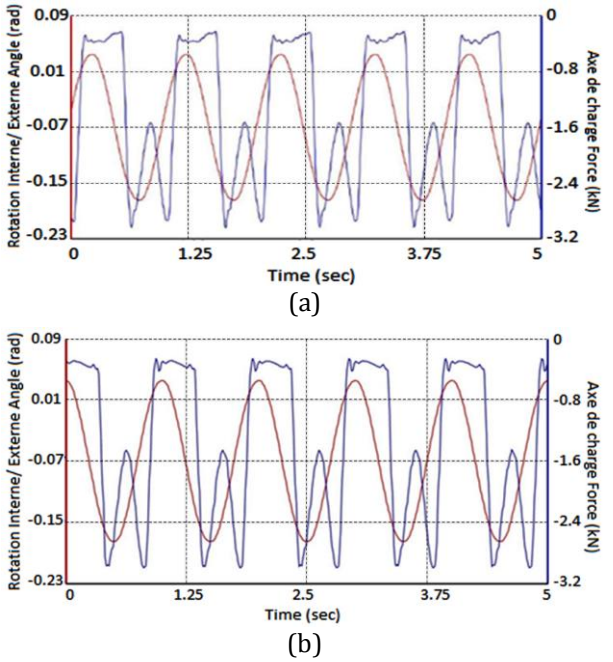

Fig. 6. In time graph of the vertical contact force and angular displacement of inner-outer rotation when testing (a) the cemented prosthesis and (b) a cementless prosthesis.

In Figure 6 is presented the graph of normal force and angular displacement in inner-outer rotation (a) when testing the cemented prosthesis and (b) cementless prosthesis.

It can be seen as a function of time graph of the vertical contact force and angular displacement command-response when testing the cemented prosthesis and cementless prosthesis, is very similar for both AA, FE, IOR.

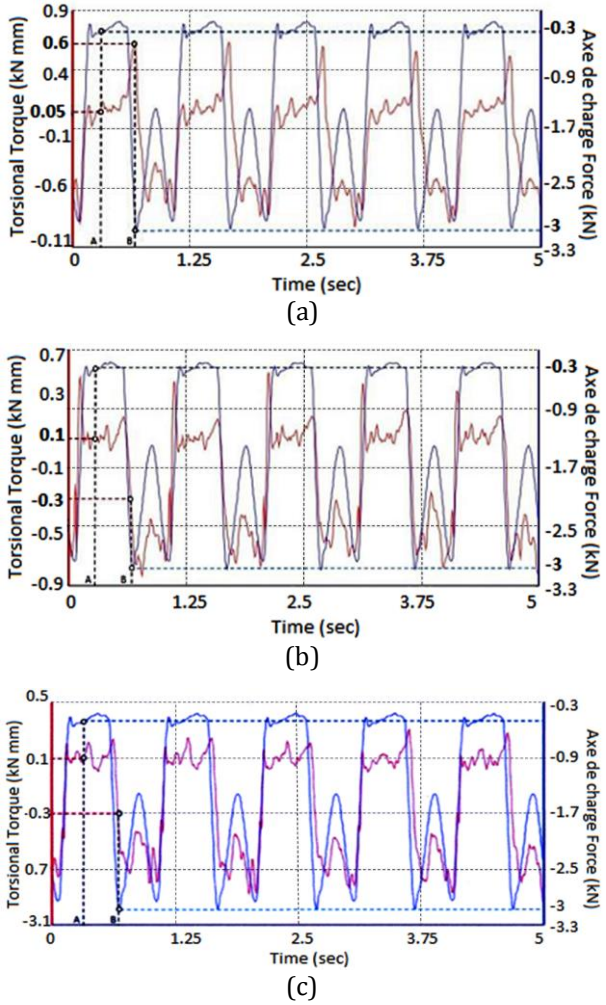

Fig. 7. In time graph of vertical contact force (blue) and of the friction torque (red), at the cemented stem testing.

Representations of Figs. 7 and 8 are very important because they show comparatively the in time variation graph of vertical contact force (blue) and in time variation graph of the friction torque (red) of cemented stem and cementless stem. These records were made at 2450000 cycles, when limits of the torque range became larger and more variable, showing that friction between the femoral head and the acetabular cup became bigger, obviously not due to wear, because the wear occurs after millions of cycles. To illustrate this, Figs. 7 and 8 show three records for each stem.

Figure 7 presents the graph of the vertical contact force and the friction torque, for the cemented stem testing.

Figure 8 shows the graph of the vertical contact force and of the friction torque, at the cementless stem testing.

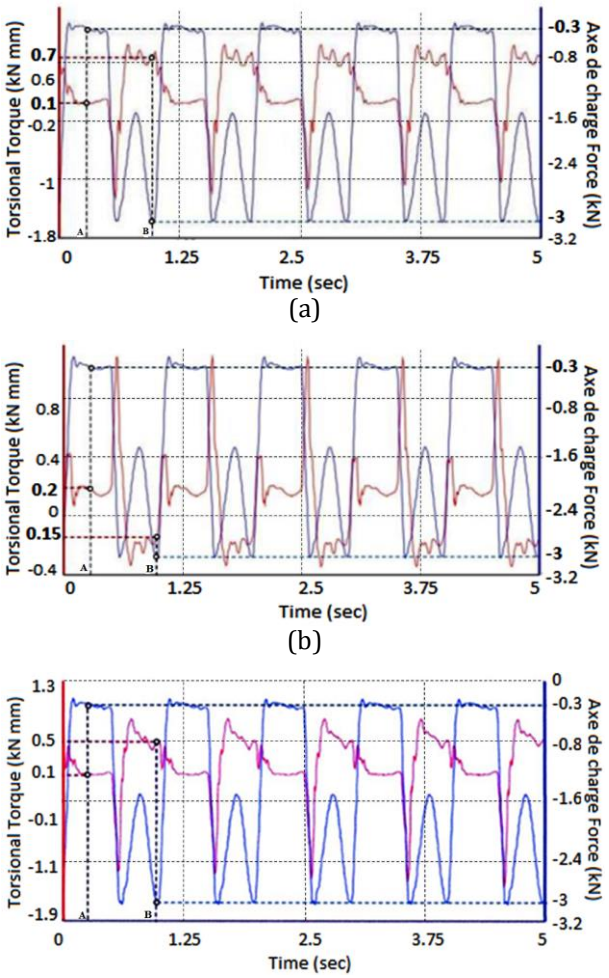

Fig. 8. In time graph of vertical contact force (blue) and of the friction torque (red), at the cementless stem testing.

In these graphs, the minimum and maximum values of the magnitudes variation represented can be observed. These values are marked on the x axis with A and B points.

The joint of the hip implant presented in Fig. 1(b) is a spherical joint with 3 degrees of freedom, which represents the three rotations around the coordinate axes (ω_x, ω_y, ω_z) – Fig. 9.

Translational constraints on the 3 coordinate axes are materializing by forces W_x, W_y, W_z. The friction moment in a spherical joint is given by the relationship:

$$M_f = \mu RW. \quad (1)$$

where: M_f is torsional moment of friction, μ is friction coefficient, R is the joint radius (in the case of the femoral head of 28 mm, R = 14 mm = 0.014 m), W is the resultant of forces W_x, W_y, W_z from joint (mean the normal contact force on the joint), whose values have been set to minimum 0.3 kN and maximum 3 kN.

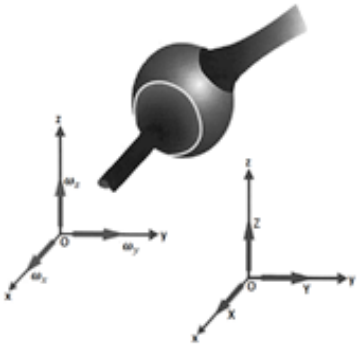

Fig. 9. Degrees of freedom of rotation and translational movement restrictions imposed by the spherical joint in Figure 1(b).

Table 7. Values of friction torque and calculated friction coefficient for cemented stem.

Graph	Point	W (kN)	M (kNmm)	μ
Fig. 7(a)	A	0.3	0.1	0.0238
	B	3	0.3	0.0072
Fig. 7(b)	A	0.3	0.05	0.0119
	B	3	0.6	0.0143
Fig. 7(c)	A	0.3	0.1	0.0238
	B	3	0.3	0.0072
Average value of the mean friction coefficient				0.0147

Table 8. Values of friction torque and calculated friction coefficient for cementless stem.

Graph	Point	W (kN)	M (kNmm)	μ
Fig. 8(a)	A	0.3	0.1	0.0238
	B	3	0.7	0.0167
Fig. 8(b)	A	0.3	0.1	0.0238
	B	3	0.5	0.0119
Fig. 8(c)	A	0.3	0.1	0.0715
	B	3	0.5	0.036
Average value of the mean friction coefficient				0.0253

On the basis of the presented graphs, Tables 7 and 8 summarize the values of friction torque recorded and of the calculated mean friction coefficient in testing of the cemented stem of the hip prosthesis, compared to cementless hip implant testing, at 2450000 cycles.

It appears that when testing the cemented stem the medium value of global friction coefficient (μ = 0.0147) is less than in the cementless implant (μ = 0.0253).

The relatively high difference between the maximum and minimum value of friction torque, and the visual observation of prosthesis functioning by transparent support fixing it, appeared to be a sign of the fretting wear manifestation. The testing was stopped when this difference occurred, at 2450000 cycles, and the prosthesis has been removed from Instron® device.

Stem prosthesis was easily extracted from the composite bone support, after some left-right movements, together with much of the PMMA cement mantle. Figure 10 shows images of both sides of the cemented stem prosthesis with a part of cement mantle, extracted after 2450000 cycles, from Instron® device.

Fig. 10. The sides of the cemented stem prosthesis together with a part of the cement mantle, extracted after 2450000 cycles of fatigue test, from Instron® device.

PMMA cement mantle was carefully removed from the femoral stem to preserve as much as possible its integrity. The stem and PMMA mantle were separately optically inspected and photographed.

Obvious corrosion of the femoral stem surface beneath the cement mantle, and reddish Fe_2O_3 deposits on the femoral stem surface and, by

transfer, on the inner part of the PMMA mantle were observed. These are due to fretting corrosion.

In Fig. 11 are shown photographic images of contact sides of the Ti6Al4V femoral stem and of the PMMA mantle, after fretting experiment.

(a) (b)

Fig. 11. Contact sides appearance of cemented stem (a) and cement mantle (b), extracted after 2450000 cycles of fatigue test, from Instron® device.

The recovered Ti6Al4V stem and interior cement mantle were further inspected by optical microscopy, hoping to identify specific cracks of fretting fatigue. The inspection proved to be very difficult due to the shape with grooves of the femoral stem and in replica, of the inner surface of the PMMA mantle. In this situation it could not be used only a Mini Handheld Digital Microscope CELESTON® #44302, with 15-30x magnification. Despite these difficult conditions, very interesting images (Fig. 12) of the femoral stem surface after fretting experiment were recorded.

They emphasize the existence of some obvious cracks on the stem surface – Fig. 12(a) and of a PMMA thin interface on the stem surface – Fig. 12(b). The interface seems to have acted as a replica film, which shows the cracks that appear to be due to internal forces induced by fretting in the stem material. Fretting stress imposes to a localized volume under the surface, very complex and non-proportional triaxial fatigue stresses.

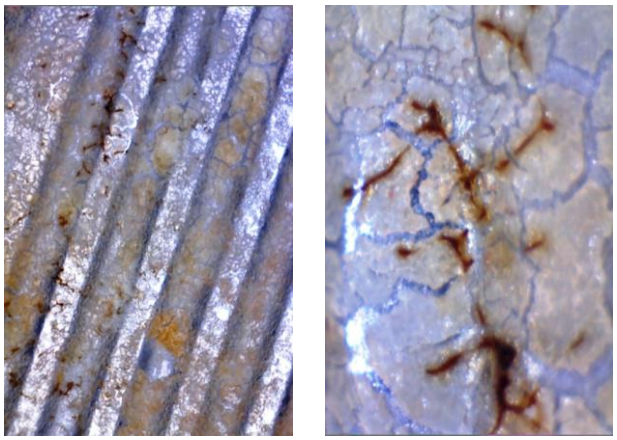

(a) (b)

Fig. 12. (a) Optical image of the femoral stem surface after fretting experiment and (b) an x30 image of a core of fretting corrosion cracks.

Images in Figures 13 indicate that the prone gradient of the fretting effort allows the crack to propagate to the surface, slowing or stopping its spread in depth.

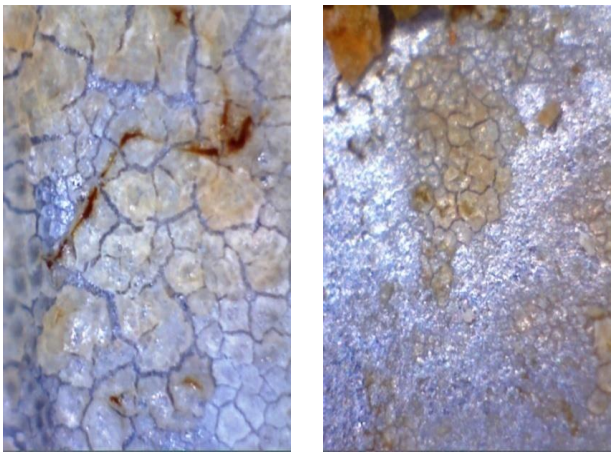

(a) (b)

Fig. 13. Microscopic images (x30) of the stem – cement mantle interface after the fretting fatigue test.

Also, Figs. 12(b) and 13 suggest that growth of fretting cracks seems to be trans-granular and this observation suggests that cracks growth can be influenced by the crystallographic structure of the stem's material. This observation is consistent with studies of D. B. Garcia and A. F. Grandt Jr. [12].

4. CONCLUSION

Fretting behaviour of the cemented femoral stem fixation of a Ti6Al4V/ UHMWPE total hip prosthesis was studied, trying to capture the loss

of contact between the femoral stem made of Ti6Al4V alloy and PMMA cement fixation. To have a landmark, the studies were performed comparatively with cementless fixation, where no fretting phenomenon occurs. The study was done on real prostheses, under biological 3D loading and motion conditions.

It was used a Instron® device for fatigue testing of the femoral stem cemented fixation of the total hip prosthesis, installed on a MTS Bionix servo-hydraulic triaxial dynamic testing machine. It allowed both monitoring the flexion-extension, abduction-adduction and inner-outer rotation movements, and the variation of the torsional torque, depending on normal loading.

Ti6Al4V alloy was immersed in a solution having a high concentration of NaCl (~ 0.2 M) at a temperature of 38 °C.

Because of the significant difference in mechanical properties (Young's modulus, with a ratio of 90 between Ti6Al4V and PMMA) shielding stress occurs. This physical phenomenon can be explained by the fact that the metallic material and polymer do not present the same deformation under the applied stress, leading to unsoldering between the metal and cement. Therefore, the adhesion between metal and polymer loses after a short period.

This unsoldering involves the fretting and subsequent friction between materials in contact. Thereafter, Ti6Al4V and the bone cement are subjected to small displacements, friction loadings in a corrosive environment, resulting in fretting corrosion. Consequently, the wear between the bone cement and Ti6Al4V alloy occurs, involving the generation of debris.

After the failure of stem fixation of cemented prosthesis at 2450000 cycles, it was visually inspected, photographic records were made, whereupon the mantle of bone cement remaining adherent on the femoral stem was removed. Visual and microscopic inspection of the femoral stem and of the inner part of the PMMA mantle demonstrated the existence of obvious corrosion of the femoral stem surface beneath the cement mantle, Fe_2O_3 deposits on the femoral stem surface and on the inner part of the PMMA mantle.

REFERENCES

[1] M. Buciumeanu, I. Crudu, L. Palaghian, A.S. Miranda and F.S. Silva, 'Influence of wear damage on the fretting fatigue life prediction of an Al7175 alloy', *International Journal of Fatigue*, vol. 31, no. 8-9, pp. 1278–1285, 2009.

[2] K. Kim, J. Geringer, J. Pellier and D.D. Macdonald, 'Fretting corrosion damage of total hip prosthesis: Friction coefficient and damage rate constant approach', *Tribology International*, vol. 60, pp. 10-18, 2013.

[3] H. Gelb, H.R. Schumacher, J. Cuckler, P. Ducheyne and D.G. Baker, 'In vivo inflammatory response to polymethylmethacrylate particulate debris: effect of size, morphology, and surface area', *Journal of Orthopaedic Research*, vol. 12, no. 1, pp. 83-92, 1994.

[4] J. Geringer, B. Forest and P. Combrade, 'Fretting-corrosion of materials used as orthopaedic implants', *Wear*, vol. 259, no. 7-12, pp. 943-951, 2005.

[5] J. Geringer and D.D. Macdonald, 'Modelling fretting-corrosion wear of 316L SS against poly (methyl methacrylate) with the Point Defect Model: Fundamental theory, assessment, and outlook', *Electrochimica Acta*, vol. 79, pp. 17-30, 2012.

[6] N.A. Bhatti and M. Abdel Wahab, 'A review on fretting fatigue crack initiation criteria', in: *International Journal of Fracture Fatigue and Wear*, in *Proceedings of the 5th International Conference on Fracture Fatigue and Wear*, Kitakyushu, Japan, 2016, pp. 78.

[7] J. Geringer, J. Pellier, M.L. Taylor and D.D. Macdonald, 'Fretting corrosion with proteins: The role of organic coating on the synergistic mechanisms', *Thin Solid Films*, vol. 528, pp. 123-129, 2013.

[8] H.A. Fadag, S. Mall and V.K. Jain, 'A finite element analysis of fretting fatigue crack growth behavior in Ti–6Al–4V', *Engineering Fracture Mechanics*, vol. 75, no. 6, pp. 1384-1399, 2008.

[9] A.E. Giannakopoulos, T.C. Lindley, S. Suresh, and C. Chenut, 'Similarities of stress concentrations in contact at round punches and fatigue at notches: implications to fretting fatigue crack initiation', *Fatigue & Fracture of Engineering Materials & Structures*, vol. 23, no. 7, pp. 561-571, 2000.

[10] M. Nesládek, M. Španiel, J. Jurenka, J. Růžička and J. Kuželka, 'Fretting fatigue experimental and numerical approaches', *International Journal of Fatigue*, vol. 44, pp. 61-73, 2012.

[11] V. Florescu, L. Capitanu, L.L. Badita and V. Filip, 'A Novel Engineering Spherical Bearing, with Potential Application for a Hip Implant', Journal *of Mechanics Engineering and Automation*, vol. 6, pp. 217-226, 2016.

[12] D.B. Garcia and A.F. Grandt Jr., 'Fractographic investigation of fretting fatigue cracks in Ti–6Al–4V', *Engineering Failure Analysis*, vol. 12, no. 4, pp. 537-548, 2005.